SAE International

Direct Visualization of Combustion in an E85-Fueled DISI Engine under Various Operation Conditions

2013-01-1129
Published
04/08/2013

PO-I Lee, Nick Polcyn and Ming-Chia Lai
Wayne State University

doi:10.4271/2013-01-1129

ABSTRACT

Gasoline-direct-injection (GDI) engines have been adopted increasingly by the automotive industry in the recent years due to their performance, effects on the environment, and customers' demand on advanced technology. However, the knowledge of detailed combustion process in such engines is still not thoroughly analyzed and understood. With optically accessible engines (OAE) and advanced measuring techniques, such as high-speed digital imaging, the in-cylinder combustion process is made available directly to researchers. The present study primarily focuses on the effects of different parameters of engine control on the combustion process, such as fuel types, valve deactivation, ignition timing, spark energy, injection timing, air-fuel ratio, and exhaust gas recirculation. Three engine heads of a 2.0L GDI engine are used with modification to acquire different optical access. Pure (E0) and ethanol-blended (E85) gasoline are used, and the engine speed and coolant temperature are kept low to imitate start-up situations in the normal driving condition. The visualization study is realized with two high-speed digital cameras, a color one and a monochrome one with an intensifier, to capture the combustion images.

The results indicate that the engine could start up in the first cycle by injecting E85 even for coolant at room temperature. Valve deactivation operation, which usually enhances the air-fuel mixing under low load conditions, may have a negative impact due to the convection effects on spark and spray plume at starting conditions. Optimal ignition timing and higher spark energy could also improve the combustion process to reduce misfire and cycle-to-cycle variation at the low speed conditions.

INTRODUCTION

More and more automotive manufacturers are implementing GDI engines in their production vehicles. The engines are known for their drivability, power density, and fuel economy especially with downsized and down-speed operations [1].

However, to understand the entire combustion process in details requires various measurement techniques and simulation analyses [2,3,4,5,6]. In addition, there are many parameters to optimize an engine from the engine calibration and control perspectives, such as injection timing, ignition timing and energy, variable valve-train (deactivation, lift, and cam-phasing), and flexible fuel requirement, etc. With more stringent fuel economy and emission regulations, it is necessary to better understand the combustion process to simultaneously achieve the clean and high efficiency goals.

Throughout the past years, engine research and development has evolved and benefited with advanced diagnostics, among which high speed imaging with OAE is prominent because of the direct “insights” gained into the combustion chamber. With digital high speed camera, the study could be controlled more precisely in addition to faster post-processing. Many laser techniques [7,8,9] have been applied to study the combustion process from the charge preparation to the pollutant formation. However, direct visualization without the aid of lasers can still yield interesting and important insights; for example, to study the effects of mixture formation inside the engine cylinder in terms of temperature, pressure, injection timing, and variable valve-train configuration [10,11,12,13,14,15,16,17,18]. It is well known now that adequate swirl and tumble air motion will assist the mixing process, and that combustion stability could be improved with varied injection timing [19]. The literature also indicates that ethanol-gasoline blends, such as E85, have larger injection quantity and latent heat. Such blends also produce

quite different vaporization process from E0 subject to the influence of the chamber temperature and pressure. For example, E85 has been shown to have slower liquid penetration and larger gas plume than E0 at the same engine environment, and may actually improve the engine startability at low temperature [20,21,22,23].

Recently low speed pre-ignition has attracted the attention of researchers because of its randomness and impacts on engine performance and life [24,25,26,27,28,29,30,31]. Many papers have concluded that this phenomenon is caused by several factors, for example, local hot spot inside the combustion chamber, oil droplets in the air-fuel mixture, and fuel components. Direct optical access to the combustion chamber also has been shown to a useful research tool, to obtain better understanding.

Besides the above mentioned parameters, advanced spark design and operation may also impact engine combustion [32,33,34,35]. With different shapes and various discharge energy, the engine startability and combustion stability could be improved.

Therefore, the present study primarily focuses on the effects of different engine control parameters on the combustion process in terms of fuel types, valve deactivation, ignition timing, spark energy, injection timing, air-fuel ratio, and exhaust gas recirculation. The coolant temperature is easily controlled using an electric heater, yet the slightly lower coolant temperature in the current paper is set up on purpose to imitate ambient cool-start condition.

EXPERIMENT SETUP AND METHOD

Experiment Setup

There are two engine experiments in the present paper: Visualization of an OAE and that of a modified production engine. Three engine heads are used to provide different view angles into the combustion chamber. The one on the OAE is intact since optical access is provided through transparent liner or windows mounted on both sides of the metal cylinder, and transparent window mounted on top of the Bowditch piston. Two other cylinder heads are modified for the metal engine tests. Figure 1(a-1) shows that one valve is replaced with a sapphire window for optical access from the top using an endoscope through the valve stem, but is limited to valve deactivated operation. Fig. 1(a-2) shows a sapphire window plug for endoscope access, which is mounted on the side of the cylinder head to study the spark and early flame development and propagation.

Table 1 shows the specifications of the engines used in the current research. The OAE is a one-cylinder engine designed for optical access with a Bowditch piston. The advantage and purpose to use this type of engines is to gain the maximal optical access; nevertheless, larger crevice volume and blow-by is expected due to the design and oil-less lubrication, so some adjustments are made to approach the real-world conditions, e.g., longer stroke in this case. The metal engine is a production engine with three cylinder deactivated, and it provides real-world conditions during the testing with realistic crevice volume. It also has higher limit and durability on engine speed and load than the OAE. Figure 1 shows the setup of both engines. Due to the limited optical access, the visualization on the metal engine is taken by a high speed monochrome camera equipped with an. The spectral response of the color camera is shown in Fig. 2. The blue color peaks from 450 nm to 470 nm. The specifications of both cameras are shown in Table 2.

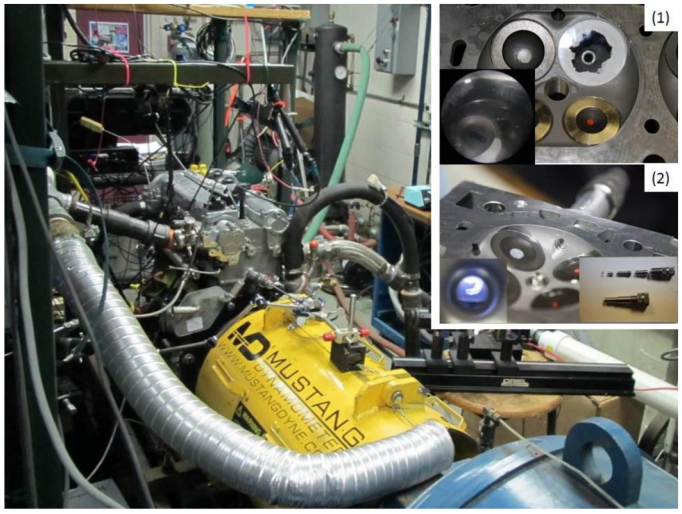

Figure 1. (a) Metal engine setup.

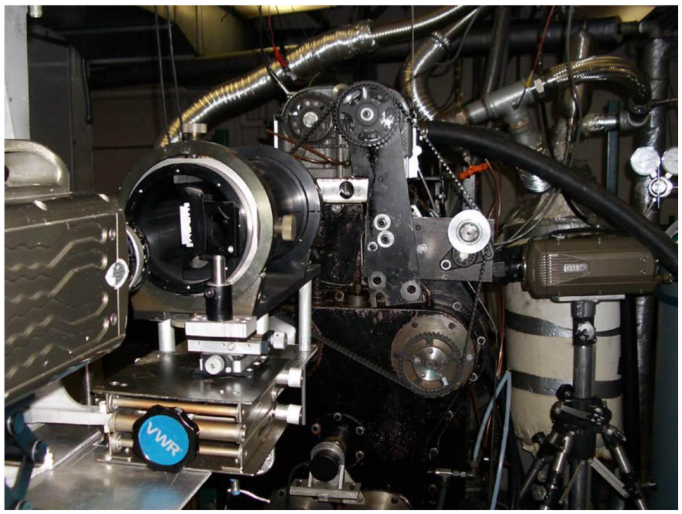

Figure 1. (b) OAE setup.

Table 1. Engine Specifications

	OAE	Metal
Displacement (L)	0.627	0.500
Bore (mm)	86	86
Stroke (mm)	108	86
Compression Ratio	10.47:1	9.2:1
Con-Rod Length (mm)	220	145
Testing Speed (RPM)	600	1200

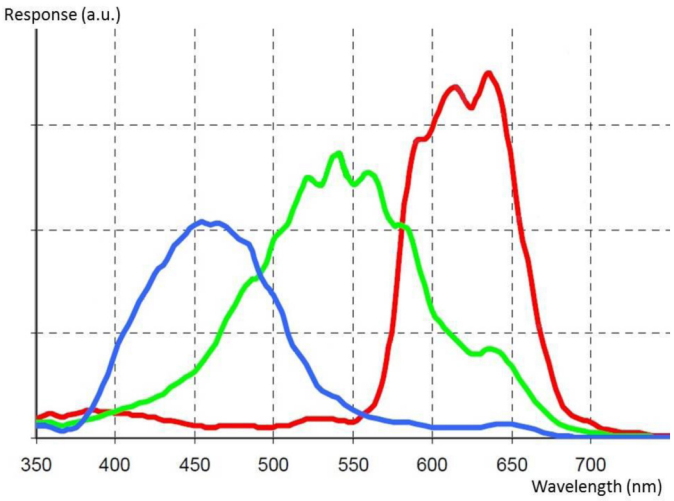

Figure 2. Color camera spectrum.

Table 2. Camera Specifications

Camera	Color	Monochrome
Phantom	V310	V7.1
RGB Response Peak	~640 nm (R) ~540 nm (G) ~450 nm (B)	N/A
Frame Rate (fps)	500k (max)	1400k (max)
Resolution (pixel * pixel)	1280 * 800 (max)	1280 * 800 (max)

Two types of fuel are used in the study: pure gasoline (E0) and ethanol-blended one (E85). A production six-hole injector is used and mounted on the intake side of the engine block. The injection pressure is fixed at 100 bar throughout all tests. Nitrogen is used to reduce the oxygen concentration and reduce window fouling due to combustion products, so that only the dilution effects of the external EGR are simulated. For the metal engine, natural gas burner exhaust is introduced at the intake to simulate external EGR and also to reduce the window fouling.

Due to the variation of the experimental setup in this paper, the detailed baseline operating conditions, such as lambda and injection timing, will be listed in the result discussion.

Test Procedure

All experiments are done by the following two test procedures with respect to the engine types due to different types of control systems. The OAE test is to measure the very first cycles once the ECU is on; the metal engine one is to acquire reasonable data statistically since it has better durability. These procedures are considered as pseudo-steady state since the actual testing period is less than 1 min. The discrepancy between the two procedures is due to the geometric differences of the two engines. The combustion will not occur for the study otherwise.

OAE Test

1. Warm up the engine by heating up the coolant and inlet air to 80 °C and 40 °C, respectively.

2. Motor the engine at 600 rpm.

3. Start the injection, ignition, camera recording, and data acquisition right after the engine speed is reached.

Metal Engine Test

1. Warm up the engine with a coolant heater until the coolant temperature reaches 40 °C. Air temperature is as the room temperature, which is about 25 °C.

2. Start the engine at 1200 rpm.

3. Start camera recording and data acquisition if the combustion is stable.

The tests are conducted according to the following parameters (not in the testing order):

- Fuel type
- Valve deactivation
- Spark timing and engine speed
- EGR
- Air-fuel ratio (presented as lambda, no specific test)
- Injection timing
- Spark discharge energy

Valve deactivation is shown in Fig. 3 as one-valve deactivation and no-valve deactivation. The images are taken from the OAE during the intake valve opening. All bottom-view results in the current paper use the setup shown in Fig. 3. The intake valves are at the bottom of the images with the deactivated one on the right hand side from the readers' view, and the exhaust ones are on the top.

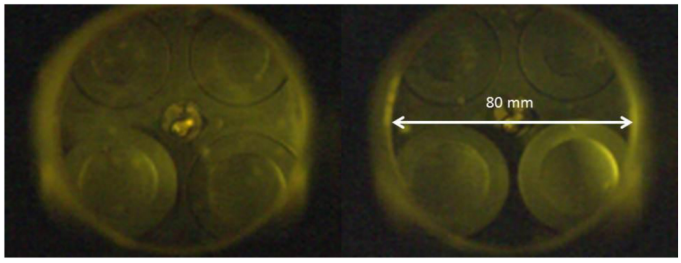

Figure 3. (a) Left: one-valve deactivation. (b) Right: no-valve deactivation.

RESULTS AND DISCUSSION

Fuel Type

E0 Flame Speed

Test condition:

- 600 RPM
- MAP: 1 bar
- Injection timing: 300 CAD $bTDC_{fire}$
- Injection pressure: 180 bar
- Ignition timing: 30 CAD $bTDC_{fire}$
- Lambda: ~1.63
- EGR 0%
- Frame Rate: 6000 fps

Figure 5 shows the image results of E0 combustion starting from the first cycle. The images present that the first cycle is relatively weaker than the successive ones; even though the combustion is observed, the flame speed data, normalized with the mean piston speed and shown in Fig. 5, indicates that the first cycle has a very slow flame propagation. Once the surrounding is developed, as seen in Fig. 4(b), the images show higher intensity, and the flame propagates faster as the results shown in Fig. 5. Qualitative flame progression is shown in Fig. 4(c). This test is done in lean condition, so the flame is expected to be faster if the air-fuel mixture is richer. It should be addressed that this test is separately from other tests mentioned later in the paper, so there is no comparison should be made.

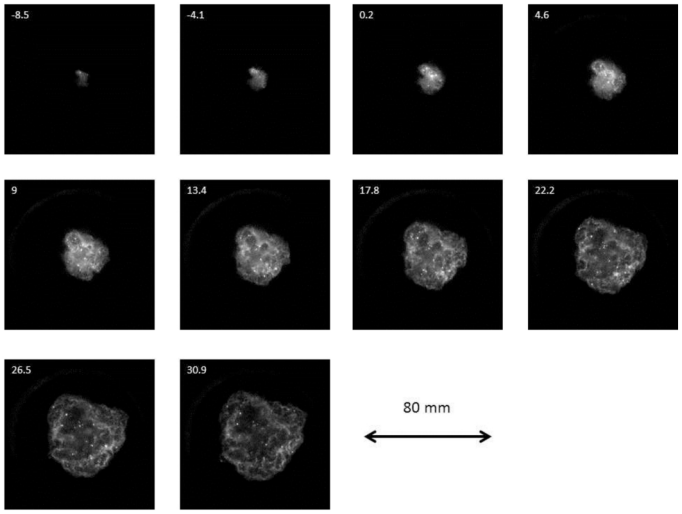

Figure 4(a). E0 combustion at 1st cycle.

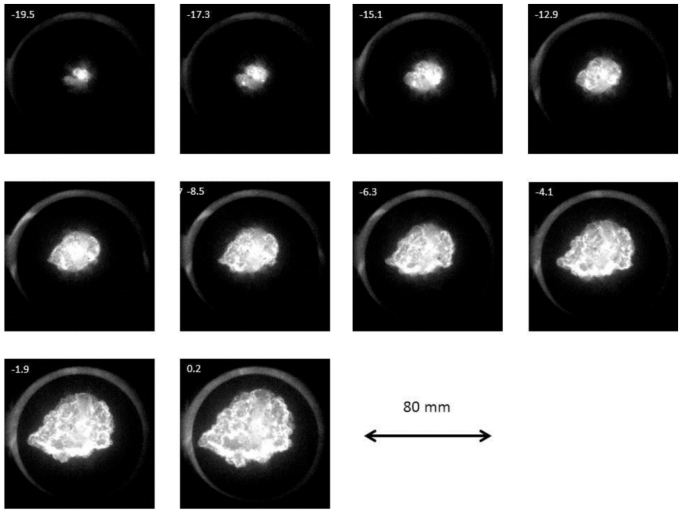

Figure 4(b). E0 combustion after 1st cycle (5th cycle shown).

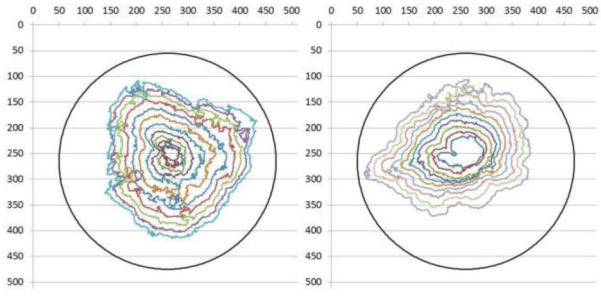

Figure 4(c). E0 flame contour at 1st cycle (left) and 5th cycle (right). The axes are in pixel.

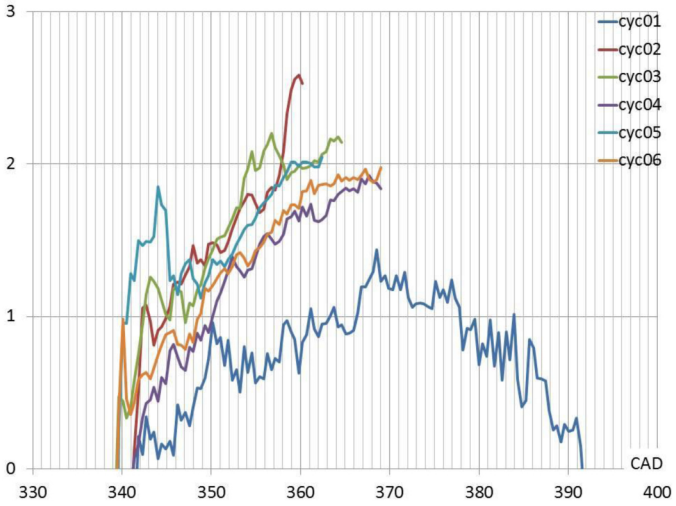

Figure 5. E0 flame speed of the first six cycles (Y-axis: normalized with the mean piston speed).

E0 v.s. E85

Test condition:

- 600 RPM
- MAP: 1 bar
- Injection timing: 180 CAD $bTDC_{fire}$
- Injection pressure: 100 bar
- Ignition timing: 45 CAD $bTDC_{fire}$
- Lambda: ~1.63 (E0) and ~1.58 (E85)
- EGR 0%
- Frame Rate: 6000 fps

The images of E0 and E85 combustion are shown in Fig. 6(a) and Fig. 7 along with their RGB values, respectively. The injection started at 180 CAD $bTDC_{fire}$ to signify the difference between E0 and E85 in this test. The averaged IMEP of E0 is 3.72 bar, and that of E85 is 4.51 bar; the coefficient of variation (COV) of the IMEPs is 47.76% for E0 and 6.81% for E85.

Even though most modern optical research involves laser technology, such equipment is very expensive and requires a lot of maintenance, which may not be financially practical. Therefore, the researchers of the current study utilize the color information obtained directly from the camera as the tool for combustion analysis. RGB value is calculated according to Eq. 1.

$$RGB_{average} = \frac{\sum_{i=1}^{i=n}(Red,Green,or\ Blue\ Value)}{Area_{effective}} \quad (1)$$

$RGB_{average}$: the averaged red, green, or blue value of a raw image calculated by Eq. 1

Red, Green, or Blue value: the value of a pixel of a raw image based on 16-bit unsigned integer (uint16); the value could vary from 0 to 65535

$Area_{effective}$: the area of an image where the actual combustion chamber is shown; only the pixels in the area are calculated

i = 1…n: the i^{th} pixel in the effective area; 1 is the first one and n is the last one

There is no combustion recorded in the first cycle of E0, so the images of the ensuing cycles are shown in Fig. 6(a). It is evident that E85 provides much stronger and more stable combustion than E0 does because the RGB values in Fig. 7 are higher than those in Fig. 6(a).

The first cycle of E85 is relatively weak comparing with the ensuing cycles. However, E85 provides better startablity since there is no combustion in the first cycle using E0. This is because that ethanol has lower boiling temperature than most of the heavy components of E0, and there is more fuel vapor available for ignition since more E85 fuel is injected than E0 to compensate its lower energy content. The trend may be reversed at even lower ambient temperature when not enough heat in the charge air is available to vaporize the fuel.

It should be noted that the blue values have similar magnitude between all cycles and the two types of fuel. In Fig. 7, it is seen that the peak of the apparent heat release rate (AHRR) coincides with the blue color. The correlation is not as strong for the E0 case in Fig. 6(a), but the start of the blue color and AHRR still occur at the same time. This may indicate that the blue flame, which is representative of the lean flame, is correlated to the flame propagation and responsible of most of the heat release.

Comparing the images at −15, 0, and 15 CAD in Fig. 6(a) and 7, it is shown that blue color starts and peaks earlier than the red one, with the green one in between, indicating richer pockets in the later combustion processes, where soot burn-out is taking place. Higher peak pressure is observed for E85 cases than E0 ones because of more complete combustion. Due to better startability, the ensuing experiments are conducted with the utilization of E85 on both the OAE and metal engine.

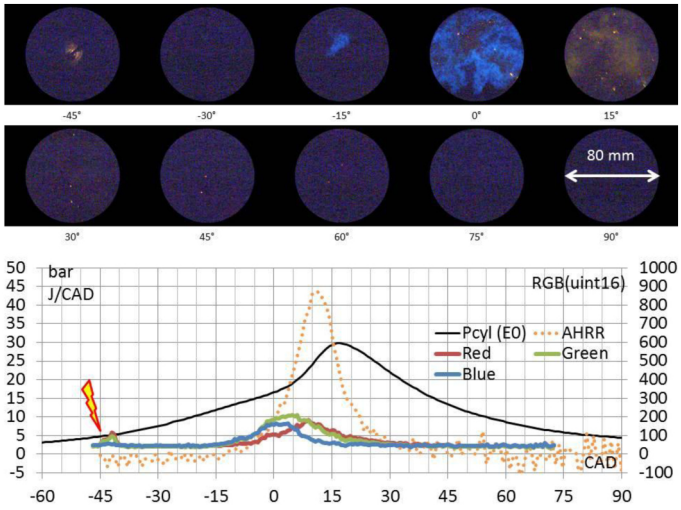

Figure 6(a). E0 combustion after 1st cycle (5th cycle shown).

Figure 6(b) shows two spectra of the E0 combustion, one at TDC_{fire} and the other one at 15 CAD aTDCfire. It is seen that OH* exists through the period of combustion; however, CH2O and CH may be covered by the stronger chemiluminecent light from CO-O. The reference wavelength is compared according to [36]. From Fig. 2 it is known that the blue color from the high speed camera is from 375 nm to 575 nm, so it may partially present some combustion products.

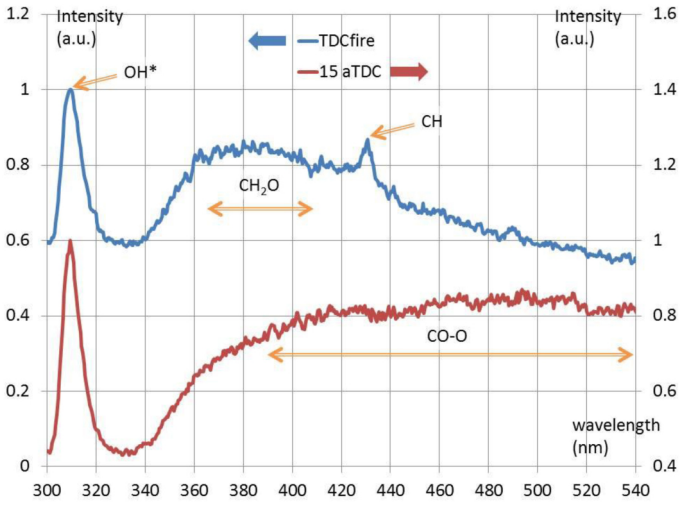

Figure 6(b). Spectra of E0 combustion at TDC_{fire} and 15 CAD $aTDC_{fire}$.

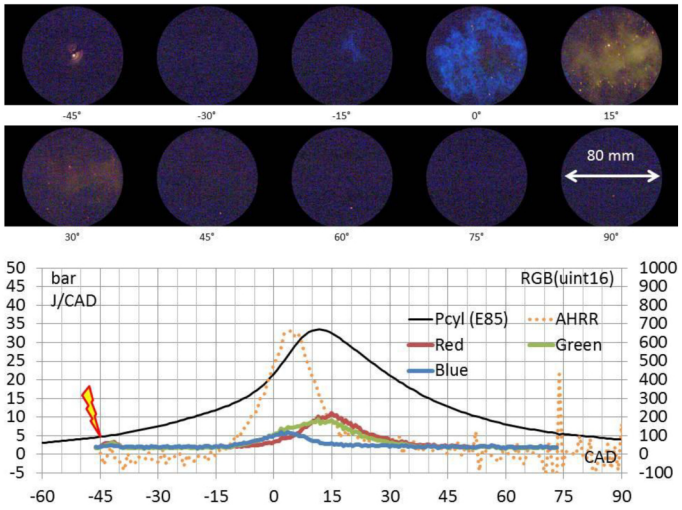

Figure 7(a). E85 combustion (1st cycle).

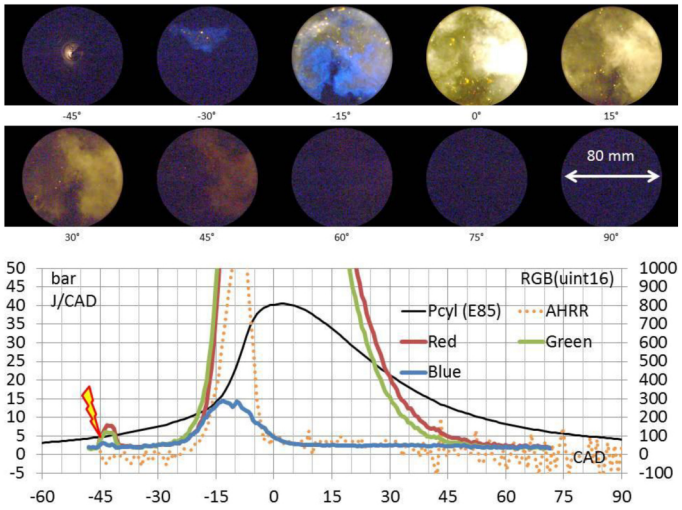

Figure 7(b). E85 combustion after 1st cycle (5th cycle shown).

Valve Deactivation

Test condition:

- 600 RPM
- MAP: 1 bar
- Injection timing: 300 CAD $bTDC_{fire}$
- Injection pressure: 100 bar
- Ignition timing: 30 CAD $bTDC_{fire}$
- Lambda: ~1.20 (E85)
- EGR 0%
- Frame Rate: 6000 fps

This test is experimented with E85 as discussed in the previous section. Theoretically, one-valve deactivation creates more swirl motion (swirl-dominant) inside the cylinder due to asymmetric intake air flows, whereas no-valve deactivation has more tumble motion (tumble-dominant) caused by the piston reciprocation. Figure 8 and 9 show the first cycle images of these to modes, no-valve and one-valve deactivation, respectively.

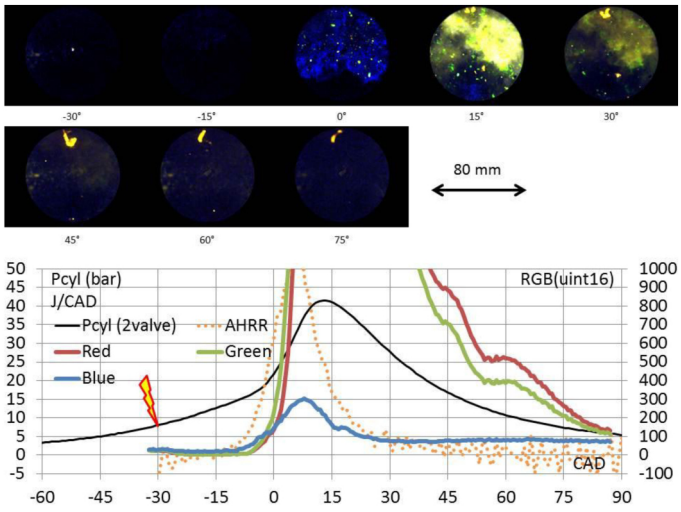

Figure 8. No-valve deactivation (1st cycle).

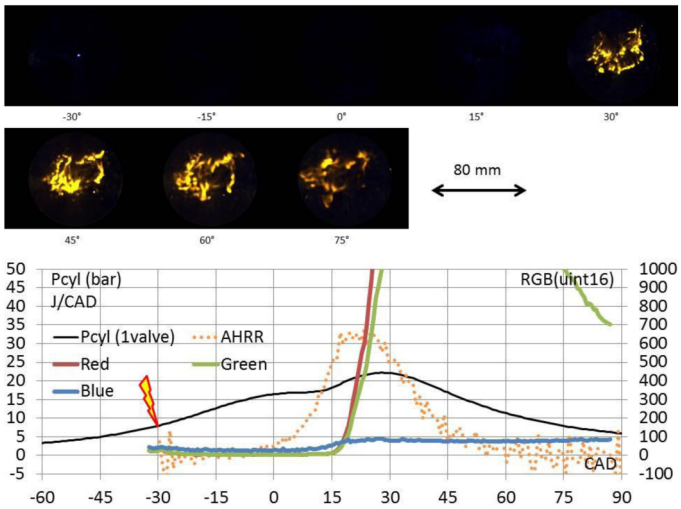

Figure 9. One-valve deactivation (1st cycle).

The first cycle of one-valve deactivation has relatively weak combustion, as shown in Fig. 8. On the other hand, the combustion of the first cycle of no-valve deactivation is stronger. Since E85 is the only fuel utilized in this test and its good combustibility is discussed and proven previously, the results indicate the impact of one-valve deactivation on deteriorating the combustion process in this particular engine setup because the IMEP of the first cycle of no-valve deactivation and one-valve deactivation is 6.88 bar and 5.52 bar, respectively. It is also observed that the combustion process is weaker with one-valve deactivation from the AHRR and RGB values. In addition to that, one-valve deactivation images show strong diffusional flame at the end of the combustion. It is therefore expected that the soot formation is higher with this configuration.

The correlation between the blue color and AHRR also agrees with the observation from the fuel type tests. The peaks of both curves overlap with each other, which indicate that the blue color may be burn rate related. It is also worthy of notice that the averaged blue values are mostly the same in any tangible combustion, but the averaged red values always vary from cycle to cycle depending on the combustion.

Nevertheless, the averaged IMEP of no-valve and one-valve deactivation is 6.58 bar and 6.82 bar; the COV of them are 3.91% and 6.87%, respectively. This suggests that even though the combustion is slightly stronger with one-valve deactivation, it is more stable while no valve is deactivated.

In order to study the difference between these two valve configurations, an ultra-lean condition (lambda ~ 1.6) with early spark timing (45 CAD $bTDC_{fire}$) is conducted in order to focus on the blue flame propagation. The image results shown in Fig. 10(a) and (b) are compared side-by-side from the start of ignition (15 CAD $bTDC_{fire}$) to the TDC_{fire} (0 CAD). It should be noted that the RGB values of the images in Fig. 10(a) and (b) are enhanced, so they should not be compared with the images in Fig. 8 and Fig. 9.

The flame kernel of one-valve deactivation starts from the bottom-right to the top-left of the image; the flame kernel of no-valve deactivation starts from the top to the bottom of the image.Figure 10(c) is the image data taken from the one-valve deactivated cylinder head on the metal engine for qualitative study. Comparing Fig. 10(b) and (c), the flame development before TDC (0 CAD) should be seen as the blue flame. Both figures show the same flame development direction, so the shape of piston top is concluded to have minimal impacts. It should be mentioned that the two tests in Fig. 10(b) and (c) are set up with the same spark plug at different ignition timing; nonetheless, both results show the same flame development direction.

From Fig. 3 it is known that the bottom of the image is the intake valve position and the top of that is the exhaust valve position. Therefore, the flame propagation is directed by the air flow motion where one-valve deactivation is dominated by swirls and no-valve deactivation is controlled by tumbles.

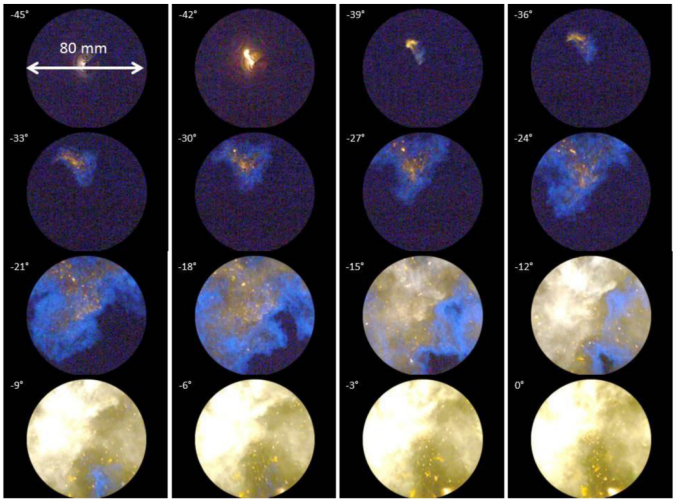

Figure 10(a). No-valve deactivation flame development.

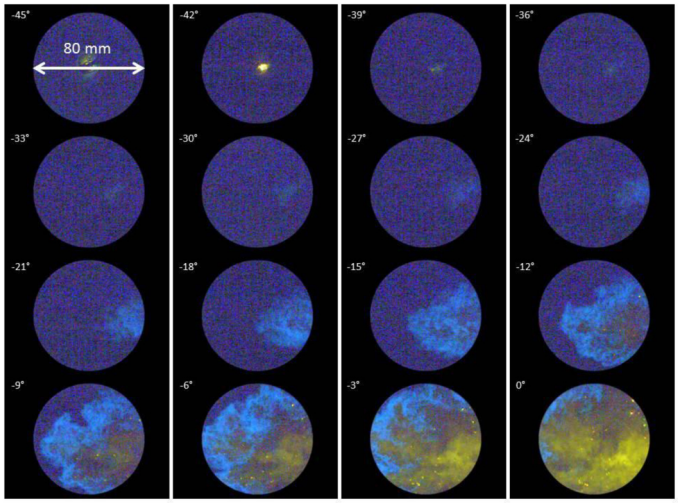

Figure 10(b). One-valve deactivation flame development.

One explanation of this phenomenon is that the direction of the spark discharge arc does not encounter a local-rich zone. A CFD simulation is done to display the air-fuel ratio inside the combustion chamber before the spark. The result is shown in Fig. 11. It is clear seen that the local-rich zone occurs at the activate intake valve side while the arc is moving towards the deactivated valve. Therefore, the control of the spark arc direction is important in order to encounter a local-rich zone to have better combustion.

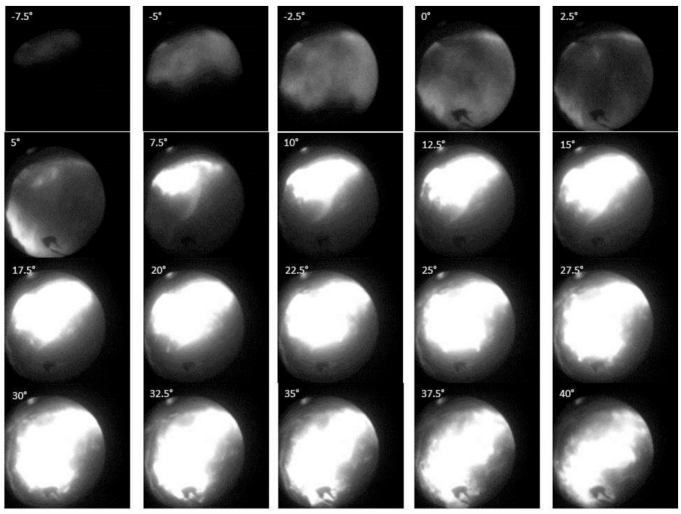

Figure 10(c). One-valve deactivation flame development in the metal engine (600 rpm; view from intake valve).

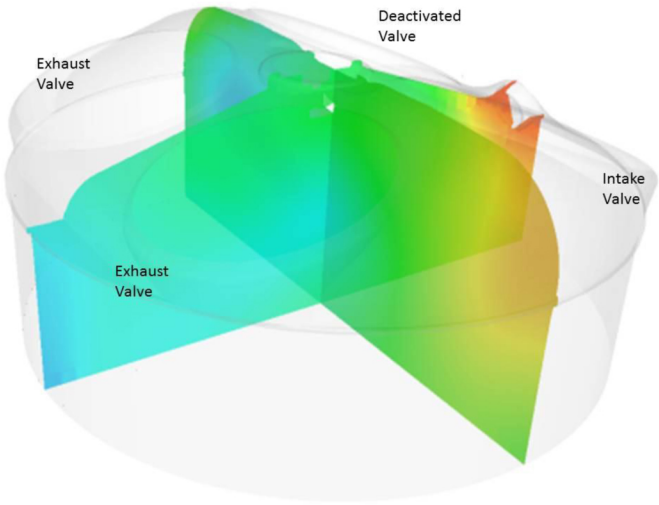

Figure 11. One-valve deactivation CFD simulation. Local-rich zone is shown in red.

Ignition Timing v.s. Engine Speed

Test condition:

- 600 RPM and 1200 RPM
- MAP: 1 bar
- Injection timing: 300 CAD $bTDC_{fire}$
- Injection pressure: 100 bar
- Ignition timing: 40 to 15 CAD $bTDC_{fire}$ (600 RPM) and 30 to 10 CAD $bTDC_{fire}$ (1200 RPM)
- Lambda: ~1.21
- EGR 0%
- Frame Rate: 6000 fps

Figure 12 shows the IMEP, CA00-10 and CA10-90 of the ignition timing sweep tests from the OAE. The test is done at lean condition (lambda ~ 1.21) with the injection at 300 CAD $bTDC_{fire}$. The spark timing is set from 40 CAD $bTDC_{fire}$ to 15 CAD $bTDC_{fire}$ on the OAE at 600 rpm, and 30 CAD $bTDC_{fire}$ to 10 CAD $bTDC_{fire}$ on the metal engine at 1200 rpm. There is no valve deactivation so that the combustion could maintain the stability.

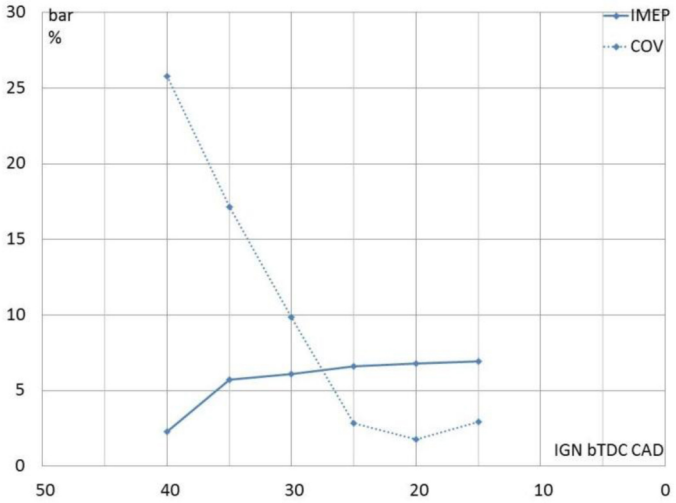

Figure 12(a). IMEP of ignition timing sweep (OAE; 600 rpm)

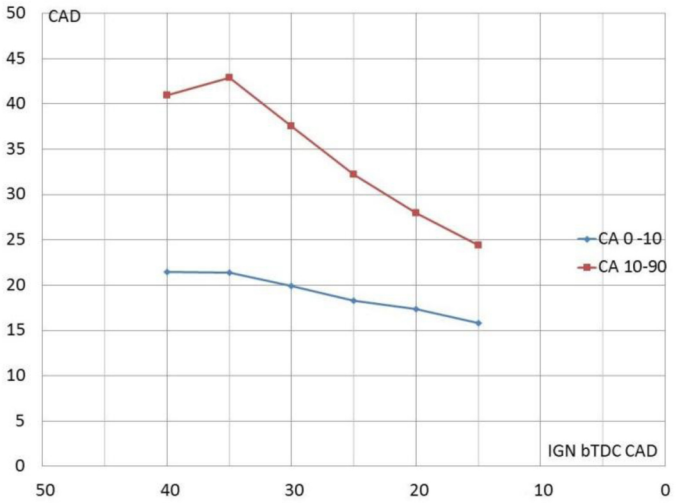

Figure 12(b). CA0-10 and CA10-90 of ignition timing sweep (OAE; 600 rpm)

At the spark timing at 20 CAD $bTDC_{fire}$ and 15 CAD $bTDC_{fire}$, the engine has high IMEP and low COV of IMEP on the OAE at 600 rpm. This indicates that most energy input is converted to work output, i.e. higher efficiency. The maximum brake torque (MBT) is considered in this range of spark timing. However, the image results demonstrate that the retard spark timing, 20 CAD $bTDC_{fire}$ and 15 CAD $bTDC_{fire}$, have in fact darker images as shown in Fig. 13. Therefore, high luminosity may not have a strong correlation to represent IMEP in this case even though the combustion is considered strong from the images. If the spark timing is too early, like Fig. 13(a), the engine would lose power and the combustion becomes more unstable as the IMEP and COV of IMEP shown in Fig. 12(a). The CA0-10 and CA10-90 results show that early spark timing causes longer burning duration.

Since the combustion phase is shifted with the advanced spark timing, most mixture could be burnt around TDC. This may explain higher luminosity and the appearance of smoke-like plume in Fig. 13, especially with advanced spark timing. The components of the plume are not studied in the current paper, but it is under investigation to identify the actual species of the plume as the future target.

Although retarding spark timing may help to improve IMEP and reduce the negative work, Fig. 13(e) and (f) show some bright spots after TDC. This could be a concern due to possible soot formation.

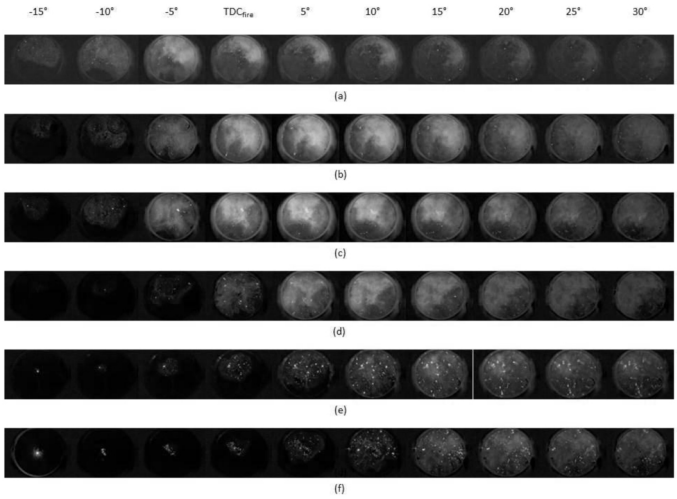

Figure 13. Ignition timing (OAE; 600 rpm): (a) 40 (b) 35 (c) 30 (d) 25 (e)20 (f)15 $bTDC_{fire}$ CAD

Ignition sweep test is also performed on the metal engine with the side-mounted endoscope. This experiment is done at 1200 rpm, which is higher than the one on the OAE (600 rpm). The IMEP and COV of IMEP results in Fig. 14(a) indicate that retarded spark timing has low IMEP and high COV, which is opposite to the results from the OAE. The MBT is reached with early spark timing. Moreover, the CA0-10 and CA10-90 data shows that the burning rate is slower with retarded spark timing in Fig. 14(b). This is also a contrast to the OAE test.

One assumption to explain the difference from these two tests is that the air motion by the piston reciprocation would impact the mixture burning rate. The CA0-10 data of early spark timing in both tests shows a flat line, which means the early flame development is not changed with respect to the

spark timing - an indication that air is not compressed sufficiently to affect the chemical reaction.

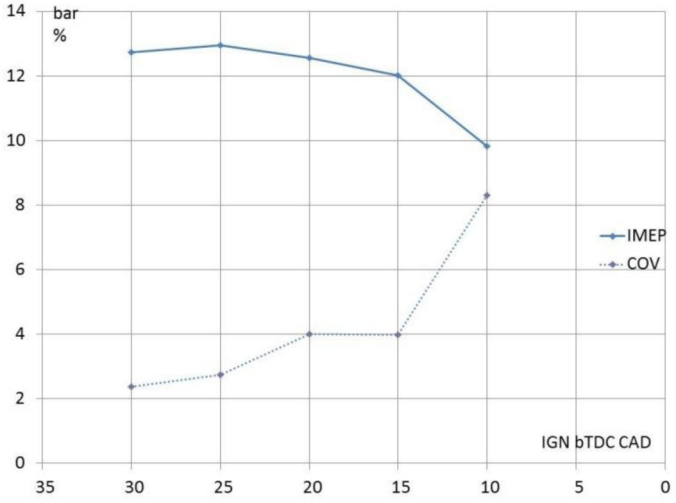

Figure 14(a). IMEP of ignition timing sweep (metal; 1200 rpm)

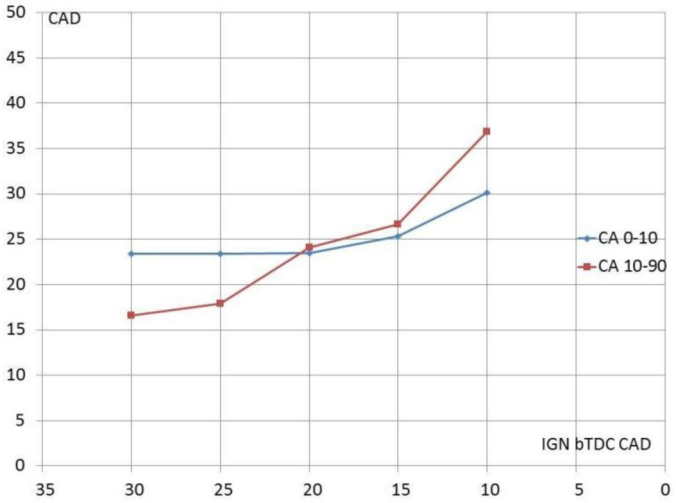

Figure 14(b). CA0-10 and CA10-90 of ignition timing sweep (metal; 1200 rpm)

Once the spark timing is retarded, CA0-10 could be faster or slower depending on the engine speed. It is believed that the flame kernel of retarded spark timing has enough time to develop at low speed, so the burning rate is faster. On the other hand, higher engine speed does not provide enough time for the flame kernel to develop thoroughly if the spark timing is retarded; thus, the combustion is deteriorated. It should be noticed that CA0-90 at 600 rpm and 1200 rpm is about 40 CAD at the MBT point, but the burn rate at 1200 rpm is actually faster due to the higher engine speed.

The image results in Fig. 15 support the assumption described above. Figure 15(a) and (b) show very robust combustion, but the chemiluminescent light is not seen much in Fig. 15(c) and (d).

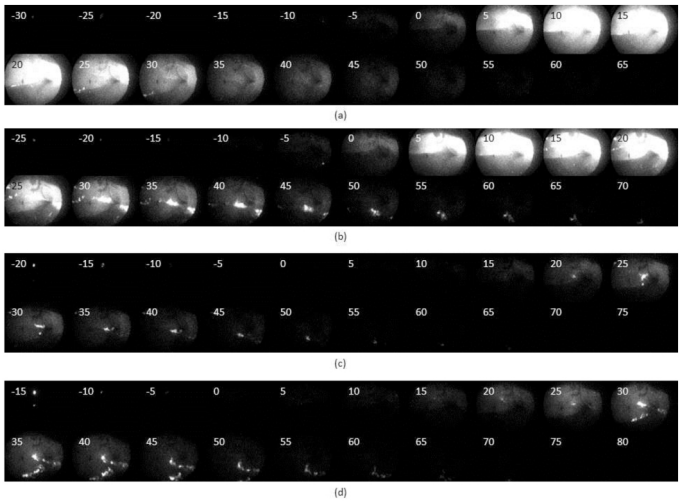

Figure 15. Ignition timing (metal; 1200 rpm): (a) 30 (b) 25 (c) 20 (d)15 bTDC$_{fire}$ CAD

Injection Timing

Test condition:

- 1200 RPM
- MAP: 1 bar
- Injection timing: 300 or 60 CAD bTDC$_{fire}$
- Injection pressure: 100 bar
- Ignition timing: 20 CAD bTDC$_{fire}$ or 10 CAD aTDC$_{fire}$
- Lambda: ~1.15
- EGR 0%
- Frame Rate: 12000 fps

Injection timing is critical in GDI engines because air and fuel need time to mix with each other. If injecting too late, the mixture will not form uniformly enough and heterogonous combustion could happen. Two cases are studied for injection timing effect: injection at 300 CAD bTDC$_{fire}$ (baseline) and 60 CAD bTDC$_{fire}$ in stoichiometric condition with 20 CAD bTDC$_{fire}$ spark timing and throttled intake. Due to possible instability concern, the tests are only performed on the metal engine. The baseline results are shown in Fig 16.

Early injection gives the air and fuel enough time to mix more homogeneously. The IMEP of the case is 13.055 bar, and CA50 is at an optimal position, which is 5 to 10 CAD aTDC$_{fire}$. However, once the injection is retarded to 60 aTDC$_{fire}$, as shown in Fig. 16(b), the combustion images indicate that the mixture does not have the same mixing quality. The flame is more heterogonous or diffusion-like.

IMEP fluctuates more with late injection, and possible pre-ignition or misfire may also occur.

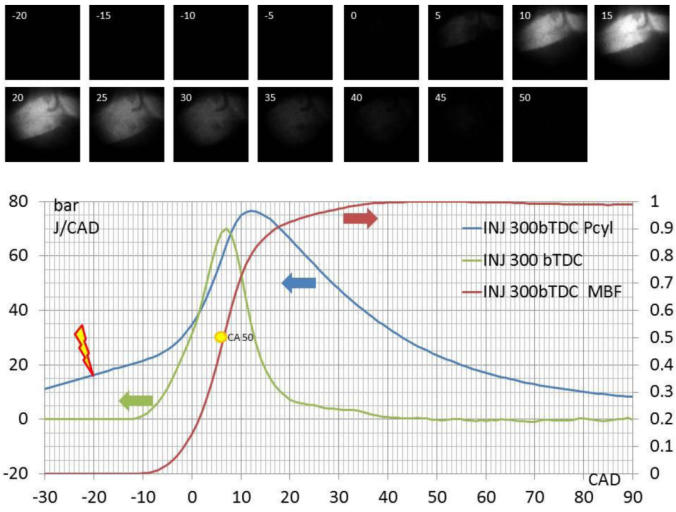

Figure 16(a). Early injection (baseline; 300 CAD $bTDC_{fire}$)

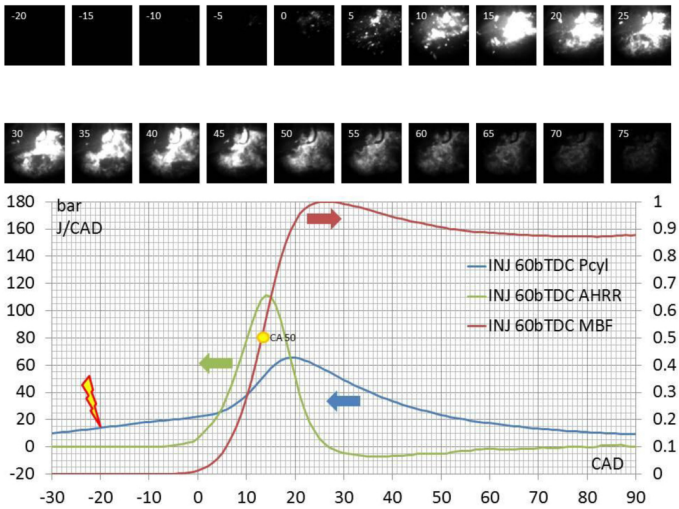

Figure 16(b). Late injection (60 CAD $bTDC_{fire}$)

Misfire and Pre-Ignition

One noticeable phenomenon of late injection is misfire. From the results of data acquisition, misfire occurs very often with late injection, whereas no misfire is observed with early injection. With the optical access, the authors compare the pressure traces and images side-by-side and discover that once a misfire occurs, the ensuing cycles have the pattern of late-burn to fast-burn. Due to the resolution of data acquisition, the results do not indicate any abrupt pressure rise, excessive peak pressure, or pressure trace fluctuation. Nevertheless, low speed pre-ignition is captured with retarded spark timing as the results shown below.

Figure 17 shows the result of a late-burn cycle, which occur right after a misfire cycle. The images show some visible flame at later CAD. To cause pre-ignition after a late-burn cycle, one hypothesis is considered that the hot burnt gas does not have time to cool down before exiting from the exhaust valves, so the residuals remain higher-than-normal temperature. Once the following cycle starts, the air-fuel mixture is warmed up faster that a fast-burn cycle would therefore occurs as shown in Fig. 18.

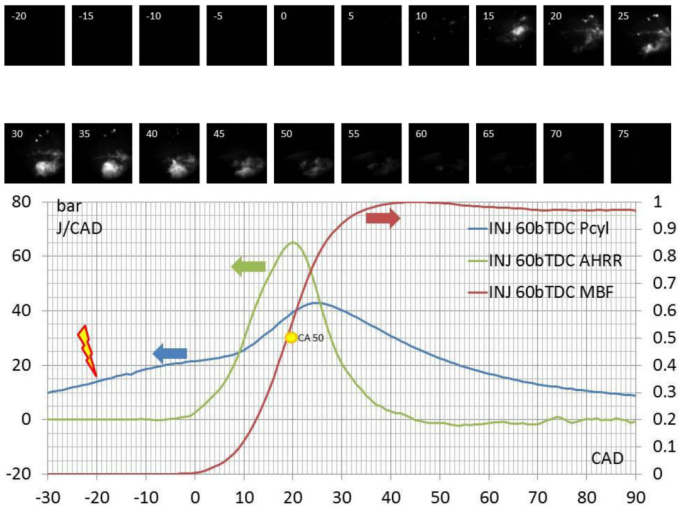

Figure 17. Late burn after a misfire

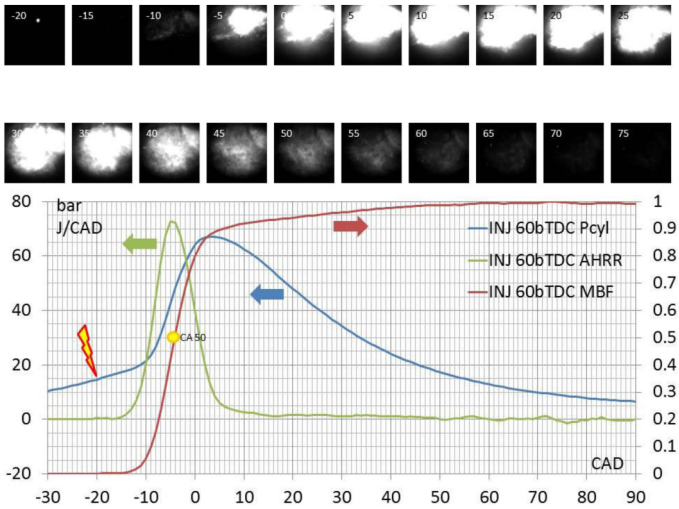

Figure 18. Fast burn after a late burn

To confirm the assumption above, the spark timing is set at 10 CAD $aTDC_{fire}$ to cause pre-ignition. Although the pressure traces of all cycles are not shown in the paper because of its complexity, it is found that a pre-ignition cycle occurs after a late-burn one. Figure 19 shows the pre-ignition image results and the pressure traces of the pre-ignition and the normal combustion. It is clearly seen that the pre-ignition combustion starts much earlier than the actual spark timing.

The first hump of the normal pressure trace in Fig. 19 could be considered as the motoring pressure trace due to late spark timing; therefore, the pre-ignition pressure trace suggests that there be endothermic reactions between −60 CAD and −30 CAD. The reactions could be due to fast vaporization process of E85, which is injected at −60 CAD. The reason for the fuel to vaporize rapidly is that there may be hot residual inside the combustion chamber from the previous cycle. Therefore, the pre-ignition occurs without the spark. Nonetheless, more in-depth research is needed to further understand the onset of pre-ignition.

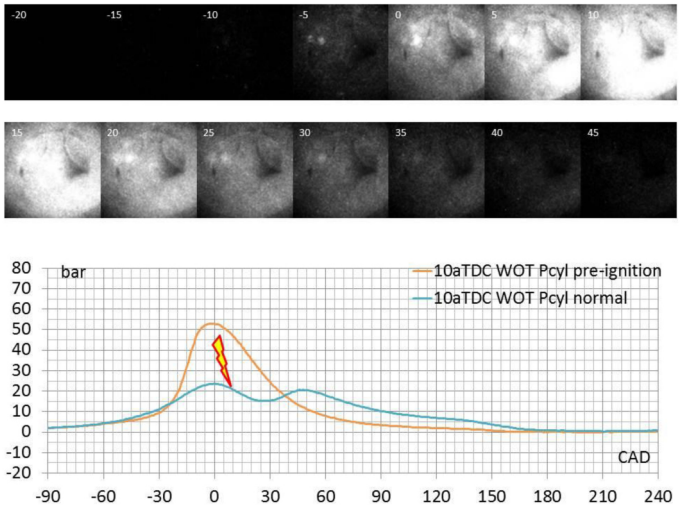

Figure 19. Pre-ignition v.s. normal pressure trace

Spark Energy

Test condition:

- 1200 RPM
- MAP: 0.5 bar
- Injection timing: 300 CAD $bTDC_{fire}$
- Injection pressure: 100 bar
- Ignition timing: 20, 15, and 10 CAD $aTDC_{fire}$
- Lambda: ~1.15
- EGR 0%
- Frame Rate: 8000 fps

The production coil of the current engine has the maximum output of approximately 50mJ (based on bench test). The authors utilize a specially made device to generate different spark discharge energy to study the impact on engine combustion. The main variables of the ignition process were initial energy discharge and arc duration. The test results show that increasing the energy could improve the combustion in a pro-misfire operating condition. Figure 20 shows the results of IMEP and COV of IMEP where improvement is achieved specifically in COV. It should be noticed that even though 4 coils (4 series) and 8 coils (4 parallel) do not show much difference in IMEP, there is an improvement in COV of IMEP with the latter.

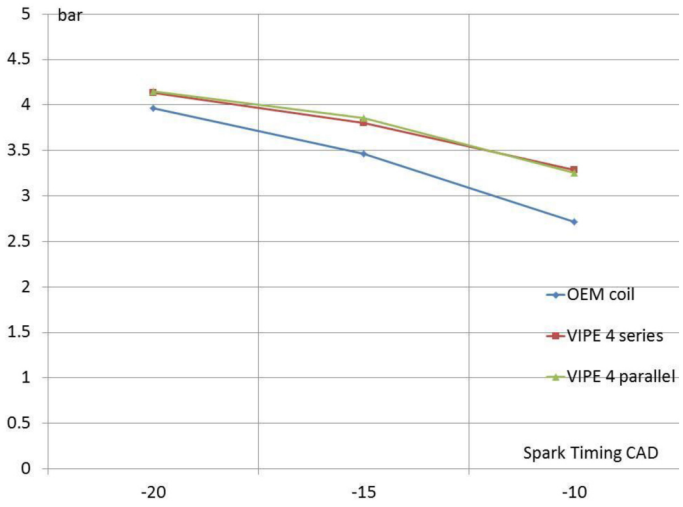

Figure 20(a). Spark energy on IMEP

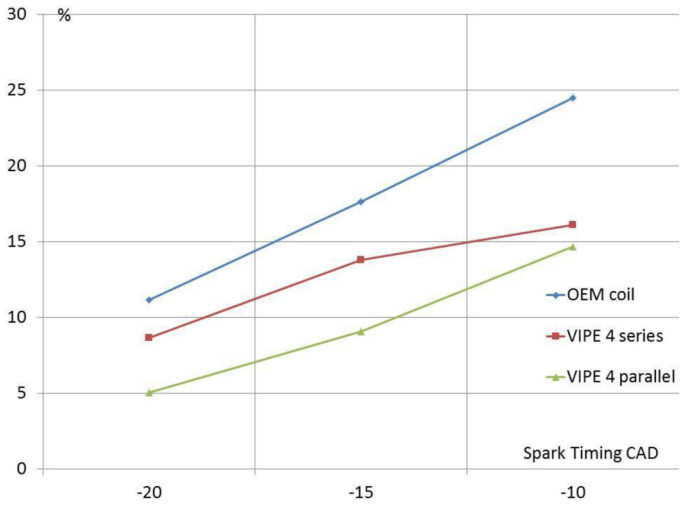

Figure 20(b). Spark energy on COV of IMEP

Figure 21 shows the image results of early flame kernel development and the radii of different coil combinations with spark timing at 10 CAD $bTDC_{fire}$. It is clearly seen that the flame kernel size is larger with more coils. Therefore, higher spark energy produces stronger flame kernel and may have faster flame propagation, which would improve combustion as the results shown in Fig. 20. Due to the proprietary issue, the exact spark energy could not be given in the present study.

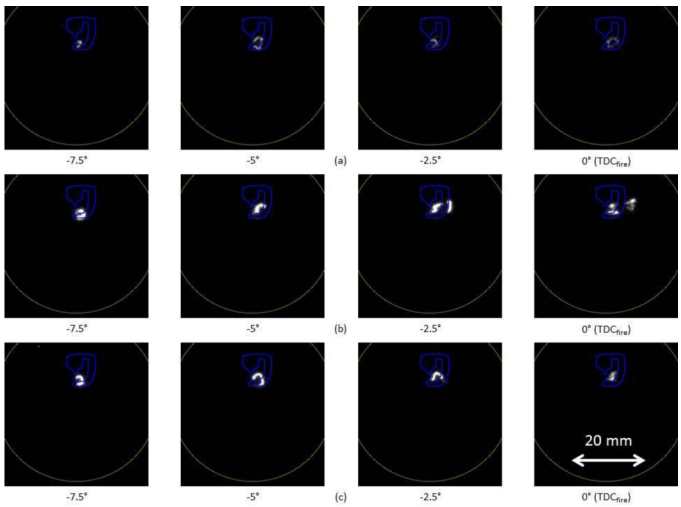

Figure 21(a). Flame Kernel Development with Different Spark Energy: (a) 1 parallel (2 coils); (b) 4 parallel (8 coils); (c) 4 series (4 coils)

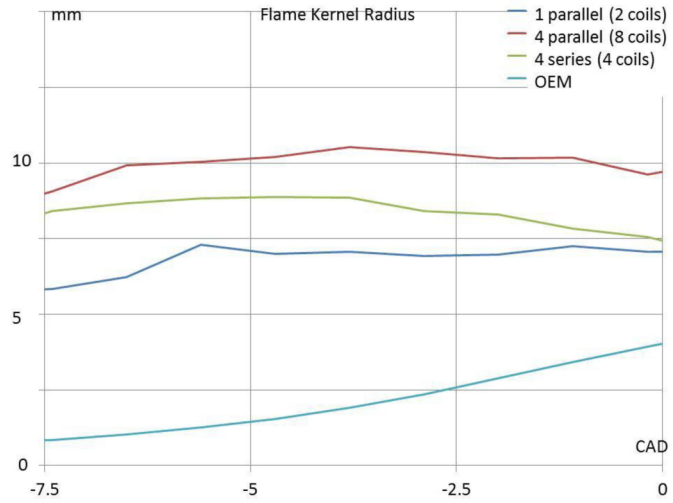

Figure 21(b). Flame Kernel Radius with Different Spark Energy

EGR

Test condition:

- 600 RPM
- MAP: 1 bar
- Injection timing: 300 CAD bTDC$_{fire}$
- Injection pressure: 100 bar
- Ignition timing: 20 CAD bTDC$_{fire}$
- Lambda: ~1.20 (lean) and ~0.9 (rich)
- EGR: 0%, 10%, 20%, and 30%
- Frame Rate: 6000 fps

Although EGR is usually not present in start-up procedure, it is interesting to see its effects on combustion with respect to the air-fuel ratio. Figure 22 shows the in-cylinder pressure traces of implementing EGR at the intake. It should be noticed that N_2 is used as EGR in the current study. The peak pressure decreases as the increment of EGR as well as IMEP. The effect of changing combustion phase by using EGR is emphasized more in Fig. 22(b) with rich condition.

Images of two cases are compared, whose spark timing is at 20 bTDC$_{fire}$. Figure 23 shows 10% EGR and 30% EGR in rich condition. The image results clearly show the difference, where 30% case shows no smoke-like plume but some bright spots. The authors believe that these local spots would result in soot formation. Furthermore, the increase of EGR would also decrease the stability of combustion, which could be verified with COV of IMEP (not shown). Therefore, unlike the prevalence of diesel engines with high EGR application, the usage of EGR needs to be studied more in GDI engines.

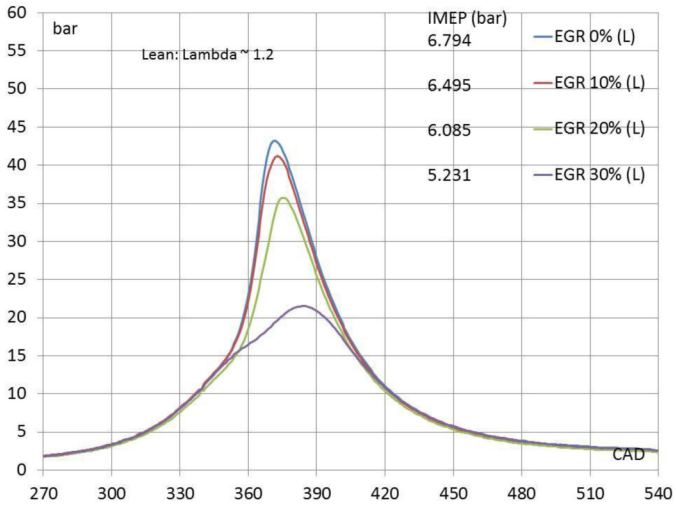

Figure 22(a). EGR effect on in-cylinder pressure (lean)

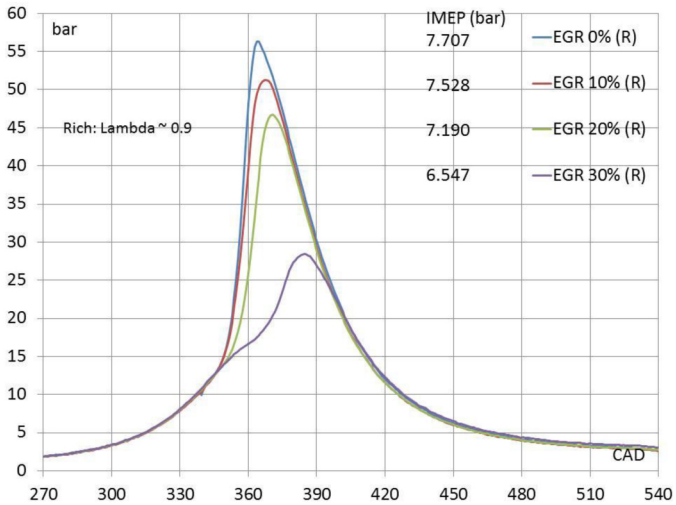

Figure 22(b). EGR effect on in-cylinder pressure (rich)

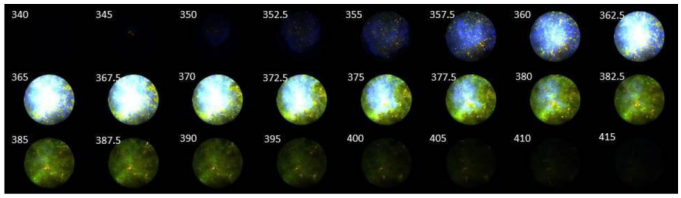

Figure 23(a). 10% EGR (rich)

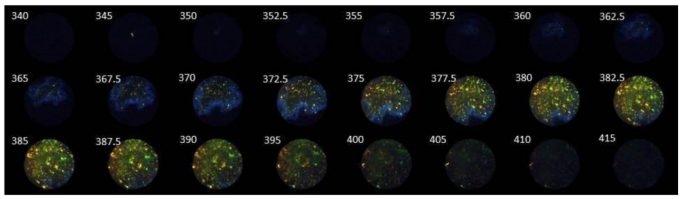

Figure 23(b). 30% EGR (rich)

SUMMARY/CONCLUSIONS

The present study primarily focuses on the effects of different parameters of engine control to the combustion process, such as fuel types, valve deactivation, ignition timing, spark energy, injection timing, air-fuel ratio, and exhaust gas recirculation. Three engine heads of a 2.0L GDI engine are used with modification to acquire different optical access. Pure (E0) and ethanol-blended (E85) gasoline are used, and the engine speed and coolant temperature are kept low to imitate start-up situations in the normal driving condition. The visualization study is realized with two high speed cameras, monochrome with an intensifier and color, to capture the combustion images.

The results indicate the following conclusions.

• The engine could have better startability using E85, with no misfire in the first cycle at low temperature; although sometimes it might cause pre-ignition after a misfire occurs, as indicated by the image and pressure data.

• Valve deactivation which usually enhances the air-fuel mixing at low load condition, may have a negative impact on the starting process and combustion stability as well as the soot formation.

• Higher spark energy could improve the combustion process and reduce misfire and cycle-to-cycle variation.

• The blue value of the color camera could represent the blue flame as well as AHRR.

REFERENCES

1. Zhao, F., Harrington D.L., and Lai, M.-C.D., "Automotive Gasoline Direct-Injection Engines," SAE International, Warrendale, PA, ISBN 978-0-7680-0882-1, 2002.

2. Alkidas, A. C. "Combustion Advancements in Gasoline," Energy Conversion and Management 48 (2007): 2751-61, doi: 10.1016/j.enconman.2007.07.027.

3. Drake, M. C., and Haworth, D. C., "Advanced Gasoline Engine Development Using Optical Diagnostics and Numerical Modeling," Proceedings of the Combustion Institute 31 (2007): 99-124, doi: 10.1016/j.proci.2006.08.120.

4. Samuel, S., Morrey, D., Whelan, I., and Hassaneen, A., "Combustion Characteristics and Cycle-By-Cycle Variation in a Turbocharged-Intercooled Gasoline Direct-Injected Engine," SAE Technical Paper 2010-01-0348, 2010, doi: 10.4271/2010-01-0348.

5. Alden, M., Bood, J., Li, Z., and Richter, M., "Visualization and Understanding of Combustion Processes Using Spatially and Temporally Resolved Laser Diagnostic Techniques," Proceedings of the Combustion Institute 33 (2011): 69-97, doi: 10.1016/j.proci.2010.09.004.

6. Tornatore, C., Sementa, P., and Merola, S. S., "Optical Investigations of the Early Combustion Phase in Spark Ignition Boost Engines," Proceedings of the Institution of Mechanical Engineers, Part D: Journal of Automobile Engineering 225 (2010): 787-800, doi: 10.1177/2041299110394915.

7. Bessler, W. G., Hofmann, M., Zimmermann, F., Suck, G., et al., "Quantitative in-Cylinder NO-LIF Imaging in a Realistic Gasoline Engine with Spray-Guided Direct Injection," Proceedings of the Combustion Institute 30 (2005): 2667-74, doi: 10.1016/j.proci.2004.08.123.

8. Katharina, K.-H., Barlow, R. S., Alden, M., and Wolfrum, J., "Combustion at the Focus: Laser Diagnostics and Control," Proceedings of the Combustion Institute, 30 (2005): 89-123, doi: 10.1016/j.proci.2004.08.274.

9. Gessenhardt, C., Zimmermann, F., Schulz, C., Reichle, R. et al., "Hybrid Endoscopes for Laser-Based Imaging Diagnostics in IC Engines," SAE Technical Paper 2009-01-0655, 2009, doi: 10.4271/2009-01-0655.

10. Kano, M., Saito, K., Basaki, M., Matsushita, S. et al., "Analysis of Mixture Formation of Direct Injection Gasoline Engine," SAE Technical Paper 980157, 1998, doi: 10.4271/980157.

11. Hung, D., Zhu, G., Winkelman, J., Stuecken, T. et al., "A High Speed Flow Visualization Study of Fuel Spray Pattern Effect on Mixture Formation in a Low Pressure Direct Injection Gasoline Engine," SAE Technical Paper 2007-01-1411, 2007, doi: 10.4271/2007-01-1411.

12. Adomeit, P., Weinowski, R., Ewald, J., Brunn, A. et al., "A New Approach for Optimization of Mixture Formation on Gasoline DI Engines," SAE Technical Paper 2010-01-0591, 2010, doi: 10.4271/2010-01-0591.

13. Matsumoto, A., Moore, W., Lai, M., Zheng, Y. et al., "Spray Characterization of Ethanol Gasoline Blends and Comparison to a CFD Model for a Gasoline Direct Injector," *SAE Int. J. Engines* 3(1):402-425, 2010.

14. Matsumoto, A., Zheng, Y., Xie, X., Lai, M. et al., "Characterization of Multi-hole Spray and Mixing of Ethanol

and Gasoline Fuels under DI Engine Conditions," SAE Technical Paper 2010-01-2151, 2010, doi: 10.4271/2010-01-2151.

15. Lai, M., Zheng, Y., Shost, M., Xie, X. et al., "Characterization of Internal flow and Spray of Multihole DI Gasoline Spray using X-ray Imaging and CFD," SAE Technical Paper 2011-01-1881, 2011, doi: 10.4271/2011-01-1881.

16. Matsumoto, A., Zheng, Y., Xie, X., Lai, M. et al., "Interactions of Multi-hole DI Sprays with Charge Motion and their Implications to Flexible Valve-trained Engine Performance," SAE Technical Paper 2011-01-1883, 2011, doi: 10.4271/2011-01-1883.

17. Zeng, W., Idicheria, C., Fansler, T., and Drake, M., "Conditional Analysis of Enhanced Combustion Luminosity Imaging in a Spray-Guided Gasoline Engine with High Residual Fraction," SAE Technical Paper 2011-01-1281, 2011, doi: 10.4271/2011-01-1281.

18. Peterson, B., Baum, E., Bohm, B., Sick, V., and Dreizler, A., "High-Speed PIV and LIF Imaging of Temperature Stratification in an Internal Combustion Engine," Proceedings of the Combustion Institute, 2012, doi: 10.1016/j.proci.2012.05.051.

19. Moore, W., Foster, M., Lai, M., Xie, X. et al., "Charge Motion Benefits of Valve Deactivation to Reduce Fuel Consumption and Emissions in a GDi, VVA Engine," SAE Technical Paper 2011-01-1221, 2011, doi: 10.4271/2011-01-1221.

20. Stan, C., Tröger, R., Lensi, R., Martoran, L. et al., "Potentialities of Direct Injection in Spark Ignition Engines - from Gasoline to Ethanol," SAE Technical Paper 2000-01-3270, 2000, doi: 10.4271/2000-01-3270.

21. Stan, C., Troeger, R., Guenther, S., Stanciu, A. et al., "Internal Mixture Formation and Combustion - fro m Gasoline to Ethanol," SAE Technical Paper 2001-01-1207, 2001, doi: 10.4271/2001-01-1207.

22. Lee, S., Tong, K., Quay, B., Zello, J. et al., "Effects of Swirl and Tumble on Mixture Preparation During Cold Start of a Gasoline Direct-Injection Engine," SAE Technical Paper 2000-01-1900, 2000, doi: 10.4271/2000-01-1900.

23. Yamamoto, S., Tanaka, D., Takemura, J., Nakayama, O. et al., "Mixing Control and Combustion in Gasoline Direct Injection Engines for Reducing Cold-Start Emissions," SAE Technical Paper 2001-01-0550, 2001, doi: 10.4271/2001-01-0550.

24. Hamilton, L., Rostedt, M., Caton, P., and Cowart, J., "Pre-Ignition Characteristics of Ethanol and E85 in a Spark Ignition Engine," *SAE Int. J. Fuels Lubr.* 1(1):145-154, 2009, doi: 10.4271/2008-01-0321.

25. Zaccardi, J., Duval, L., and Pagot, A., "Development of Specific Tools for Analysis and Quantification of Pre-ignition in a Boosted SI Engine," *SAE Int. J. Engines* 2(1):1587-1600, 2009, doi: 10.4271/2009-01-1795.

26. Dahnz, C., Han, K., Spicher, U., Magar, M. et al., "Investigations on Pre-Ignition in Highly Supercharged SI Engines," *SAE Int. J. Engines* 3(1):214-224, 2010, doi: 10.4271/2010-01-0355.

27. Amann, M., Alger, T., and Mehta, D., "The Effect of EGR on Low-Speed Pre-Ignition in Boosted SI Engines," *SAE Int. J. Engines* 4(1):235-245, 2011, doi: 10.4271/2011-01-0339.

28. Haenel, P., Seyfried, P., Kleeberg, H., and Tomazic, D., "Systematic Approach to Analyze and Characterize Pre-ignition Events in Turbocharged Direct-injected Gasoline Engines," SAE Technical Paper 2011-01-0343, 2011, doi: 10.4271/2011-01-0343.

29. Sasaki, N., Nakata, K., Kawatake, K., Sagawa, S. et al., "The Effect of Fuel Compounds on Pre-ignition under High Temperature and High Pressure Condition," SAE Technical Paper 2011-01-1984, 2011, doi: 10.4271/2011-01-1984.

30. Zahdeh, A., Rothenberger, P., Nguyen, W., Anbarasu, M. et al., "Fundamental Approach to Investigate Pre-Ignition in Boosted SI Engines," *SAE Int. J. Engines* 4(1):246-273, 2011.

31. Sasaki, N. and Nakata, K., "Effect of Fuel Components on Engine Abnormal Combustion," SAE Technical Paper 2012-01-1276, 2012, doi: 10.4271/2012-01-1276.

32. Davis, G., Bouboulis, J., and Heil, E., "The Effect of a Multiple Spark Discharge Ignition System and Spark Plug Electrode Configuration on Cold Starting of a Dedicated E85 Fueled Vehicle," SAE Technical Paper 1999-01-2664, 1999, doi: 10.4271/1999-01-2664.

33. Lee, M., Hall, M., Ezekoye, O., and Matthews, R., "Voltage, and Energy Deposition Characteristics of Spark Ignition Systems," SAE Technical Paper 2005-01-0231, 2005, doi: 10.4271/2005-01-0231.

34. Lee, Y. and Boehler, J., "Flame Kernel Development and its Effects on Engine Performance with Various Spark Plug Electrode Configurations," SAE Technical Paper 2005-01-1133, 2005, doi: 10.4271/2005-01-1133.

35. Alger, T., Mangold, B., Mehta, D., and Roberts, C., "The Effect of Sparkplug Design on Initial Flame Kernel Development and Sparkplug Performance," SAE Technical Paper 2006-01-0224, 2006, doi: 10.4271/2006-01-0224.

36. Gaydon, A. G. The Spectroscopy of Flames. Second ed. Great Britain: Chapman and Hall, 1974.

ACKNOWLEDGMENTS

This material is based upon work partially supported by the US Department of Energy under Award Number DE-EE0003258. The technical support from Dr. Marcis Jansons, Dr. Xingbin Xie, and Mr. Xin Yu at Wayne State University is also greatly appreciated by the authors.

The Engineering Meetings Board has approved this paper for publication. It has successfully completed SAE's peer review process under the supervision of the session organizer. This process requires a minimum of three (3) reviews by industry experts.

ISSN 0148-7191

SAE Customer Service:
Tel: 877-606-7323 (inside USA and Canada)
Tel: 724-776-4970 (outside USA)
Fax: 724-776-0790
Email: CustomerService@sae.org
SAE Web Address: http://www.sae.org
Printed in USA